A manuscript to the ***Journal of Micromechanics and Microengineering***

Development of a CMOS-compatible PCR-chip: comparison of design and system strategies

Ivan Erill[1*], Susana Campoy[2], José Rus[1], Luis Fonseca[1], Antoni Ivorra[1], Zenón Navarro[1], José A. Plaza[1], Jordi Aguiló[1], Jordi Barbé[2]

[1] Biomedical Applications Group, Centro Nacional de Microelectrónica (CNM-IMB), 08193 Bellaterra, Spain
[2] Departament de Genètica i Microbiologia / Centre de Recerca en Sanitat Animal (CReSA), Universitat Autònoma de Barcelona, 08193 Bellaterra, Spain

Short title: Comparison of PCR-chip estrategies
Classification numbers: 85.85.+j, 87.15.Rn, 87.80.Mj, 87.80.Tq
Keywords: PCR-chips; PCR; DNA; analysis; chip; micro-TAS; CMOS; design; sealing; biocompatibility; optimization

---

Abstract

In the last decade research in chips for DNA amplification through the polymerase chain reaction (PCR) has been relatively abundant, but has taken very diverse approaches, leaving little common ground for a straightforward comparison of results. Here we report the development of a line of PCR-chips that is fully compatible with Complementary-Metal-Oxide-Semiconductor (CMOS) technology and its revealing use as a general platform to test and compare a wide range of experimental parameters involved in PCR-chip design and operation. Peltier-heated and polysilicon thin-film driven PCR-chips have been produced and directly compared in terms of efficiency, speed and power consumption, showing that thin-film systems run faster and more efficiently than Peltier-based ones, but yield inferior PCR products. Serpentine-like chamber designs have also been compared to standard rectangular designs and to the here reported rhomboidal chamber shape, showing that serpentine-like chambers do not have detrimental effects in PCR efficiency when using non flow-through schemes, and that chamber design has a strong impact on sample insertion/extraction yields. With an accurate temperature control (±0.2 °C) we have optimized reaction kinetics to yield sound PCR amplifications of 25 μl mixtures in 20 min and 24.4 s cycle times, confirming that a titrated amount of bovine albumin serum (BSA, 2.5 μg/μl) is essential to counteract polymerase adsorption at chip walls. The reported use of a CMOS-compatible technological process paves the way for an easy adaption to foundry requirements and for a scalable integration of electro-optic detection and control circuitry.

1. Introduction

Since the introduction of the micro-Total Analysis System (μ-TAS) concept in the early 1990's [1], the trend towards the miniaturization and integration of DNA analytical techniques in microsystems has been steady and rising. The first DNA-chip demonstrators covered a broad range of techniques and applications, such as DNA electrophoresis [2, 3], PCR [4] or massively parallel hybridization [5]. Following these early proofs of concept, the focus lies now on the integration of the aforementioned and other diverse techniques into a single DNA-chip capable of conducting complete analyses [6-9]. Since the early days of the DNA-chips field, a common area of interest has been the integration of amplification techniques on chips. Due to the special nature of the samples DNA-chips deal with (i.e. nucleic acids of biological origin), the presence of an initial amplification step is usually a fundamental prerequisite for most applications and, therefore, the ability to integrate some

* Corresponding author. Tel. +34-93-594-7700. Fax. +34-93-580-1496. E-mail address: ivan.erill@cnm.es.

sort of amplification technique (e.g. PCR) becomes essential for the miniaturization and automation of processes sought in a DNA μ-TAS.

Apart from PCR, many other amplification techniques have been developed over the years, and some of them have already been implemented at the micro-scale (e.g. ligase chain reaction [10] or strand-displacement amplification [11, 12]). However, and even though PCR presents some shortcomings for its integration on chips (e.g. temperatures that nearly reach the boiling point), the powerful filtering and amplification capabilities that are inherent to PCR, coupled with a vast set of standardized applications, still make PCR the most desirable amplification technology. Moreover, the miniaturization of PCR for its integration on chips poses by itself many advantages [13]. These were early pointed out by research in capillary hot-air driven PCR systems [14] and first demonstrated in chips some years later [4]. Essentially, the miniaturization behind the PCR-chip scheme allows the use of lower amounts of reagents, a vastly more efficient heat dissipation/transfer and a more sensitive temperature control, facts that result into faster operation and improved specificity [4, 14]. This acknowledged potential led to a spur of both academic and commercial interest in PCR-chips during the 1990's decade and resulted in a series of consecutive demonstrations of their feasibility using different approaches [4, 6, 15, 16].

Unfortunately, the divergent nature of these approaches have made the PCR-chip field an orphan in many respects, with some key issues left unaddressed or, at the most, simply acknowledged, and without a common technological ground for reference and improvement. This problem is acute because, as it happens in most μ-TAS initiatives, the implicit miniaturization of PCR for its integration on chips entails many difficulties. Among other requirements, PCR-devices call for airtight sealing methods to avoid evaporation, PCR-compatible surfaces to avoid inhibition, a precise temperature control and effective means for inserting and extracting reagents and PCR-products. Some of these underlying hurdles have been partly dealt with in the literature, whilst others remain largely unaddressed. For instance, surface biocompatibility (s.c. PCR-friendliness) has been approached twice [17, 18], but the results remain somewhat inconclusive and the mechanism of PCR-inhibition by silicon-related materials is still not fully understood [19]. Similarly, other prominent issues, like device airtight sealing or reagent insertion/extraction, have been only partly dealt with [16, 20, 21] and their remaining catches have been pointed out just lately [22, 23]. Therefore, and taking into account the multifaceted nature of the approaches (thin-film vs. Peltier heaters; acrylic tape vs. rubber gasket and mineral oil sealing) and substrates (SiO_2-passivated or silanized silicon, glass and plastics) that have been used, the task of extracting useful know-how from the literature for PCR-chip production remains challenging.

In the present work, we have developed a CMOS-compatible process for the production of silicon-glass PCR-chips and we have used this technological platform as a common ground for the comparative analysis and evaluation of the most common system and design solutions found in the literature. Temperature sensors and heaters have been implemented using a single standard polySi layer on the chip back-side and PCR-chambers and access holes have been produced using deep silicon wet etching techniques that are also compatible with CMOS processes, thus improving previous CMOS-compatible PCR-chip designs and introducing the possibility of a future integration of control and detection circuitry on-chip. Using a single technological platform, different insertion/extraction systems, heating elements and chamber designs reported in the literature have been evaluated and directly compared for the first time. Their respective problems have been identified and solutions fitted to our technological framework have been put forward, developed and validated in order to produce functional PCR-chips that take full advantage of the micro-scale environment and outperform conventional thermal cyclers.

2. Materials and methods

2.1. PCR-chips

PCR-chips were fabricated using CMOS-compatible standard photolithographic processes on 5 inches, 300 μm-thick, double-side polished <100> P-type silicon wafers, combining standard CMOS processes and CMOS-compatible deep-etch processes [19]. Two different kinds of chips (hereafter named passive and active, respectively) were fabricated. Passive chips (i.e. without integrated heating/sensing circuitry) were produced by means of the relatively simple two-side process shown in Figure 1. A dry thermal oxide (2 μm) – silicon nitride (1800 Å) bi-layer was used at both sides to define the PCR-chamber area on the front side and Ø1 mm access holes on the back side. The underlying bulk silicon was then deep etched in a two-step process by sequential immersion of each wafer side in a 25% (v/v) tetra-methyl ammonium hydroxide (TMAH) solution at 80 ºC [24]. The PCR-chamber on the front side was etched to a depth of ~175 μm, providing 18.7 μl and 25.4 μl chambers for the two kinds of chamber designs here reported (serpentine-like [152.95 x 0.7 x 0.175 mm^3] and rhomboidal chambers [29 x 5 x 0.175 mm^3] respectively, see Figure 3). Thereafter, access holes were etched on the back side until wafer perforation (~125 μm, see Figure 1b). After chemical stripping of the residual mask layers, the processed wafer was passivated anew (Figure 1c) with a dry thermal oxide layer (380 Å) to generate a homogenous PCR-friendly surface environment [16, 17, 22]. The wafer was then thoroughly rinsed and the front side of wafer was anodically bonded to a 0.5 mm-thick SD-2 (*Hoya*) or 7740 (*Pyrex*) glass wafer at atmospheric pressure, 400 ºC and 1 kV [25, 26], leading to the completed devices shown in Figure 1d.

Active PCR-chips (i.e. chips with integrated heating/sensing circuitry) were produced using a more complex technological process (see Figure 2) that has already been described [19]. First (see Figure 2a), a 4800 Å phosphor-doped (15.8 Ω/□) polysilicon layer was deposited on the back side to define inter-digitized resistor grids on top of a dry thermal oxide (0.5 μm) – silicon nitride (1800 Å) bi-layer that provided homogeneous heat radiation. Each grid consisted of an array of several parallel resistors (see Figure 3). To provide uniform heating, the heater grid was made up of 18 (6 x 1 mm^2) homogeneously distributed parallel elements with a mean resistance of 79 Ω, leading to a total parallel resistance of 4.28 Ω. Average chamber temperature sensing was accomplished with a sensor grid of 8 (7 x 0.25 mm^2) regularly interspaced sensing elements with a mean resistance of 442.4 Ω and an overall parallel resistance of 55.3 Ω. After passivation of the polysilicon resistor grids with a deposited 5500 Å silicon oxide layer, process switched to the front side, where the nitride-oxide bi-layer was patterned to define the PCR-chamber and the exposed bulk silicon was deep etched (~175 μm) by a single-side TMAH attack (see Figure 2b). A 500 Å PCR-friendly SiO_2 layer was then thermally grown on both sides of the wafer to cover the PCR-chamber surface and process switched again to the back side. Electrical contacts were defined and filled by deposition of a thick (1 μm) AlSiCu alloy [98.75:0.75:0.5] layer that was later patterned to provide external contact pads and lanes. The resulting electrical structure was insulated with a standard CMOS passivation layer (SiO_2:Si_3N_4 – 4000:7000 Å, see Figure 2c), and Ø1 mm access holes were then etched through the insulating layer and the underlying bulk silicon by means of a combined reactive-ion etching (RIE) and single-side TMAH etch. After inspection, the completed device was thoroughly cleansed and anodically bonded to a 0.5 mm-thick glass wafer (see Figure 2d).

2.2. Temperature control system

2.2.1. Control software

Chip temperature was monitored and controlled with a custom developed Labview (*National Instruments*) program that allowed independent and flexible tuning of all the involved control parameters and the easy setup of elaborated PCR protocols (e.g. initial denaturation and final extension times, cold storage holds, etc.). For precise temperature control (±0.2 ºC) and fast temperature transients (up to 15 ºC/s) the program implemented a dual hysteresis PD-PID (proportional-integrative-derivative) control that prevented the otherwise unavoidable overshooting caused by integrative terms after fast transients.

2.2.2. Data acquisition, control circuitry and elements

Data acquisition and electrical stimulation of the heat sources were carried out using a PCI-1200, 12-bit analog I/O data acquisition board (*National Instruments*) working at a 12,000 samples per second regime. Temperature sensing was carried out using three complementary sensors and their respective custom-developed 4-wire sensing circuitries. A ±1.0 ºC surface K-type thermocouple probe (*Lab Facility*) was used in initial characterization and, afterwards, as a room temperature and backup reference sensor, while a 0.01 ºC surface platinum RTD class-A 1/10-DIN Pt100 probe (*Kosmon*) probe, clamped to the Peltier cell surface with pincers (see Figure 5), was used to monitor temperatures when using external heat sources and, later, as a cross-check sensor during the initial experiments with the integrated polysilicon sensors of active PCR-chips. All sensors where calibrated by immersion in mineral oil with precision reference sensors at different temperatures, and their non-linearities were corrected by software interpolation with ITS-90 (thermocouple) and Callendar-Van Dusen (Pt100) standards. In the case of integrated polysilicon sensors, their thermal coefficient of resistivity (TCR) and their resistance/temperature response were first evaluated. The TCR was found to be 5.7×10^{-3} $ºC^{-1}$ and their resistance/temperature response extremely linear on the PCR temperature range (see Figure 5). The polysilicon sensors were then calibrated by immersion in mineral oil and their read-resistance/temperature correlation was software interpolated with a 3rd order polynomial, leading to a maximum ±0.1 ºC deviation. For heating and cooling, the driving PCI-1200 analog output was connected through a HCRN200 analog opto-coupler (*Agilent Technologies*) to a custom-designed voltage modulation driver, governed by a LM12CLK 80W power op-amp (*National Semiconductor*) and powered by a ±12 V – 10 A custom-assembled FE-17 supply (*Cebek*). The power driver output was directly connected either to a CP 1.0-127-05L 30x30x3.2 mm^3 72 W Peltier cell (*Melcor*) or to the 4.28 Ω polysilicon actuator grid of active PCR-chips.

2.2.3. System setup

Although other approaches were implemented (see below), the final setup for the PCR-chip system using external heat sources (i.e. passive PCR-chips) was essentially that depicted in Figure 4. Both the PCR-chip and the Pt100 probe were mounted on top of silicon oxide passivated 300 μm-thick base chips and clamped with custom Teflon insulated pincers. In the case of the PCR-chip, the base chip was a micro-machined negative replica of the PCR-chip back side, matching the access holes of the later and thus providing very efficient airtight sealing during operation. In turn, both base chips were located on top of a 1 mm-thick (30x30 mm^2) oxygen-free copper block, which was glued with 340 Heat-sink compound (*Dow Corning*) to the underlying Peltier cell hot side, thus limiting the temperature deviation between the center and edges of the Peltier cell surface to below -0.5 ºC. The whole assembly was ultimately mounted with 340 heat-sink compound on top of a tee-slot heat dissipater (*IMI Marston*), with pedestal supports for Teflon-covered pincers that clamped securely the chip and the Pt100 probe on their respective base chips. To improve Peltier cell temperature transients, the cold-side temperature of the Peltier cell was typically raised to 55 ºC by placing the tee-slot heat dissipater on top of a Series 1000 laboratory hotplate stirrer (*Jenway*). This set the Peltier cell in the lower end of its operational 67 ºC differential temperature range during PCR cycling (50-95 ºC) and thus maximized its transient response.

In the case of active PCR-chips, a custom device consisting of two 10 mm-thick Teflon slabs (see Figure 6) was developed to accommodate simultaneous physical support, chip sealing, fan ventilation and electrical contact to the chips. A 1.1 W – 12 V electric fan (*Sunon*) was fastened on top of the upper block to provide convection cooling through the 40x50 mm^2 ventilation window drilled on both slabs. The lower slab had a grinded base (5x10x0.5 mm^3) for chip placement, with Ø1 mm access holes for electrical contact through oxygen-free copper bars and a grinded surface for the placement of 1.02 mm-thick $Ø_i$1.27 mm NBR toric joints for chip sealing. The copper bars were mounted on Teflon insulated bases and connected to the power driver. When clamping the chip between lower and upper Teflon rectangular slabs, the toric joints tightly sealed the chip access holes, while the pressure clamped copper bars provided effective electrical contact

2.3. Cleansing, sterilization and insertion/extraction of reagents

Custom devices were fabricated in methacrilate to facilitate reagent insertion/extraction and chip cleansing (see Figure 7). The devices consisted of two methacrilate slabs clamped with Ø4 mm screws, with the lower slab having an engraved chip outline (40x10 mm^2) for chip placement. Cleansing devices had toric joint capped Ø3 mm screw-matching holes on the upper slab to provide a fixing location for Ø4 mm silicon-tube interfaces on top of the chip access holes (see Figure 7b). In insertion/extraction devices (see Figure 7c), the Ø3 mm screw-matching holes were substituted by conical holes with a 0.261º conicity angle (see Figure 7d) that tightly matched the shape of a 20-P pipette tip (*ART*), thus providing efficient means for easy sample insertion and extraction.

When chip reuse was necessary, chip cleansing was conducted with a $Ø_i$8 mm tube peristaltic pump (*Watson & Marlow*), connected to the aforementioned methacrilate washing devices. The pump provided continuous and sequential (5 minutes per reagent) rinsing with the following sequence of reagents [27]: 37% hydrochloric acid ($HCl+H_2O_2+H_2O$ – [1:1:5]), 30% ammonia ($NH_3+H_2O_2+H_2O$ – [1:1:5]), 96% ethanol, 18.2 MΩ de-ionized water; all reagents (*Pancreac*) were of analytical grade (ACS-ISO). After cleansing, the chips were dried with a N_2 flow and autoclaved at 2.2 Bar - 135 ºC for 15 min in a 118-LRV autoclave (*Matachana*). Methacrilate devices were sterilized by a double-side 20 min exposure to UV irradiation in a FLV60 laminar airflow chamber (*EuroAire*).

2.4. PCR protocols

In the course of this work, different DNA templates were used for amplification (*Salmonella typhimurium* ATCC14028 strain IS200 (~200 bp) and *iroN*-promoter regions, *Pasteurella multocida* PM25 strain *hfq-hlfX* (~4 kb) region and human p53 gene exon #7) and, consequently, different PCR-mixes and protocols were used. Nonetheless, for the bulk of the analytical work here reported, PCR experiments were carried out using as template the *Xylella fastidiosa lexA* gene promoter region (~700 bp), the PCR protocols of which are reported here. Template DNA was cloned by ligation into a pGEM®-T vector (*Promega*) and then electro-transformed into *Escherichia coli* DH5 strain competent cells for culture in TF-Ap broth [28]. Prior to PCR, the plasmid DNA was extracted following the alkaline lysis method [29]. A 310 bp amplicate region was then defined with 19-mer and 20-mer upstream and downstream primers (5'-gCgTCACgggCTgCTATTg and 5'-ggCgTTTCTCCTTCgCAgAC; *Sigma-Genosys*) and the resulting PCR-mix was as follows (for 25 µl): 17 µl milliQ H_2O, 2.5 µl 10x $MgCl_2$ Taq buffer (*Roche*), 2.5 µl 10 nM dNTPs, 1.25 µl 10 µM sense primer, 1.25 µl 10 µM anti-sense primer and 0.2 µl 3.5 U/µl Expand™ High Fidelity System Taq polymerase (*Boehringer Mannheim Corp.*). The basic PCR protocol, which was later optimized for PCR-chips, was: 95.5 ºC – 1 min, (95.5 ºC – 5 s, 62 ºC – 20 s, 72 ºC – 45 s) per 40 cycles and 72 ºC – 2 min. All PCR-chip amplifications were run in parallel to control amplifications in a Mastercycler personal (*Eppendorf*) thermal-cycler. To effectively counteract adsorption phenomena, PCR-chip amplifications were conducted with a doubled Taq concentration (0.4 µl of 3.5 U/µl per 25 µl) and a titrated amount (2.5 µg/µl) of bovine serum albumin (BSA).

2.5. Agarose gels and analysis of results

To inspect PCR products, 3% (w/v) agarose gels were molded in electrophoresis MiniSub® Cell GT casting-trays (*BioRad*). The gels were run at 110 V – 1.0 A in a 10x Tris-EDTA 0.5M / pH 8 buffer containing 0.5 µg/ml of ethidium bromide for DNA staining. PCR products were loaded with a solution containing 0.25% Bromophenol Blue (*Pancreac*) and 0.25% Xylene Cyanol (*Clonetech*) for visual inspection. After a typical ~25 min run, the gels were first visually inspected under a UVP-TM36 transilluminator (*Mitsubishi*), and the corresponding electrophoresis bands were discriminated using a ϕX174 DNA/HaeIII ladder (*Promega*) as the size reference marker. For closer and more systematic inspections, gel

shots were taken with a DC120 digital camera and DNA concentrations were gauged with Digital Science 1D software (*Kodak*), using again the ϕX174 DNA/HaeIII ladder as a concentration normalizer.

3. Results and discussion

3.1. Kinetics and biochemical optimization

The main advantage of PCR-chips over conventional systems does not arise only from their faster transients (due to reduced volumes), but also from their efficient heat transfer, which ensures that the heat source temperature is distributed almost instantly across the whole PCR-chamber [4, 13, 14, 30]. This fact can be exploited to minimize redundant hold times at the three PCR temperatures (denaturation, annealing and extension), with a lower limit imposed only by the extension rate of the Taq polymerase [14, 31]. In this work, we tested these hypotheses and we optimized PCR kinetics up to the point of reducing denaturation and annealing times to mere spikes (1 and 2 s respectively, see Figure 8) and the extension hold to 10 s. Due to the reduced denaturation times, we were also able to increase slightly the denaturation temperature (up to 96 ºC) and to extend the number of PCR cycles (up to 45) without evidence of polymerase decay. The results (see Figure 9) show that, as predicted, PCR specificity improves when annealing times are decreased, but the overall performance of the reaction seems to be negatively affected by fast cycling, producing slightly inferior products than control reactions. A feasible explanation for this effect may reside in the fact that, in conventional reactions, extended annealing takes place during the relatively slow cooling and heating transients immediately before and after the annealing hold period. Conversely, in chip PCR with very fast transients, this principle does not hold and reaction efficiency becomes hampered due to low annealing rates [14]. Therefore, to obtain yields comparable to those of standard reactions, primers must be carefully selected to ensure that effective annealing takes place during the spike-hold, and the annealing temperature must be carefully titrated to obtain optimal results. This means that reactions must be carefully targeted for fast operation and, consequently, that not all PCR reactions may be effectively adapted for fast PCR, as this will depend on the availability of suitably long and matching specific primers in the DNA region targeted for amplification. In general, these results (see Figure 9) are in agreement with previously reported amplifications in PCR-chips, although a straight comparison is difficult due to the different approaches taken in the literature. Even though slightly higher yields have been reported [4, 16, 22], these results implied either longer PCR-protocols [16, 22] and/or larger concentrations of both Taq polymerase and template DNA [4, 22], and when similar conditions have been assayed here, the PCR yields obtained are comparable to those previously reported in the literature (see Figure 13).

Compatibility of chip materials with PCR operation is obviously a fundamental issue in PCR-chips, and has been granted some thorough studies in standard [17] and flow-through PCR-chips [18]. Although silicon-related materials may play some part in direct PCR inhibition [17], recently we have shown that adsorption phenomena play the leading role in the inhibition of PCR in non flow-through silicon-based chips [19]. Adsorption phenomena are prevalent in static, rectangular-chamber PCR-chips due to their high surface-to-volume ratios [17], and they contribute to PCR-inhibition through non-specific sequestering of Taq polymerase, but of not DNA as has been previously suggested [32]. In accordance with previous findings [16, 18, 33, 34] we have also shown that the addition of titrated amounts of BSA can effectively counteract this adsorption [19]. BSA is supposed to compete with Taq polymerase for active adsorption sites, thus blocking polymerase adsorption to some degree. To achieve efficient chip PCR experiments, here we conducted titration experiments to determine the optimal BSA concentration for chip operation. This was determined to be in the whereabouts of 2.5 μg/μl, with higher concentrations (i.e. 5 μg/μl) resulting in lower yields and lower concentrations (i.e. 0.5-1 μg/μl) not fully counteracting polymerase adsorption. Nonetheless, even when using the titrated 2.5 μg/μl

BSA concentration, experiments on PCR-chips still had to be conducted with a doubled Taq polymerase concentration (0.056 U/μl) in order to achieve yields similar to those of positive controls. This effect has previously been reported [16] and is probably due to the very low polymerase concentrations otherwise used in both these works (0.028 U/μl), for which even the residual polymerase adsorption that persists under BSA blocking may be enough to hinder PCR efficiency.

3.2. Analysis of chip design alternatives

Although it has been mainly neglected in the literature, chip design, concerning mostly reservoir design, can be an important factor in many facets of PCR-chips. In this work, we focused on two particular aspects that could be influenced by reservoir design: sample insertion/extraction efficiency and PCR-friendliness. The issue of reagent insertion and extraction is of critical importance in PCR-chips, since PCR is often a preliminary step in many analytical procedures and the amplified product must be recovered for further analysis. This problem can be partly circumvented if on-chip quantitative detection [16, 35, 36], integrated hybridization [7] or integrated electrophoresis [6, 9, 37] are coupled to the chip, but these approaches impose restrictions on the range and nature of the analyses that can be applied to the amplified product. Moreover, it remains to be seen whether, in the mid term, the integrated molecular laboratory of the future will rely on complex, fully integrated fluidic systems or, else, on multi-chip module schemes assisted by existing automated sample dispensing systems. Here we examined several reported techniques for sample insertion and extraction, and we found out that the proposed schemes present many extraction problems due both to methodology and chip design.

The most intuitive way to provide sample insertion/extraction capabilities is to glue a silicone or plastic tube to the chip access holes [4, 21]. This approach was assayed here with rectangular reservoir chips (see Figure 10a), by directly gluing $Ø_i$1 mm silicon tubing to the access ports using a conventional fast glue. Leaving aside the fact that the unavoidable lateral stresses involved in chip handling frequently broke down the tube-chip bond, it was found that insertion and extraction of small volumes (20-30 μl) of sample were hindered by liquid stacking at tube walls, an effect that could not be effectively overcome by the use of a custom-devised vacuum extraction trap, leading to low insertion yields (~40%) and extremely poor extraction yields (below 10%). Simpler methodologies for sample insertion/extraction have been proposed [16, 16, 22], involving the direct placement a pipette tip on top of the access port and the application of a positive/negative pressure to insert/extract reagents. When using this approach, we found that, although sample insertion could be easily carried out and was indeed assisted by capillary effects, sample extraction posed many reproducibility problems and extraction yields were, on average, unbearably low (30-40%). With the introduction of pipette tip matching methacrilate devices (see Figure 7c-d), insertion yields were improved up to the 95-100% range, but extraction yields were raised only to a tolerable 60% by using a combined procedure that consisted of an initial suction with the pipette tip at the output port and a final positive N_2-flow pressure at the input port [17, 22]. Further examination led to the conclusion that this upper extraction limit was a direct consequence of the particular design of the PCR-chamber. The abovementioned tests had all been carried out using a rectangular reservoir design (see Figure 10a) that has been often described in the literature [15, 17], and in which access holes are located off the PCR chamber and connected to it through short capillaries. After extensive testing, we found out that the extraction limit was caused by the formation of a low-resistance air conduct between the input and output ports. In essence, once a certain amount of the inserted liquid has been extracted, the formation of an airway between input and output ports becomes practically unavoidable and, once in place, the air conduct impedes the further extraction of reagents, which remain stuck at chip walls [22]. Alternative designs [16], with access holes located on top of the PCR-chamber (see Figure 10b), were also tested here, but yielded even lower extraction yields as the airway formed earlier. Such problems had already been highlighted in the literature [22], and had been partially circumvented with a serpentine-like design of the PCR-chamber [22]; see

Figure 10c). However, since no detailed analysis of the influence of serpentine-like designs on static PCR kinetics and inhibition had been conducted to date, we resorted to a compromise solution, producing 18.7 μl serpentine-like chips and 25.4 μl rhomboidal chips (see Figure 3, Figure 10c-d) that minimized reagent stacking while still providing an ample resemblance (i.e. close surface-to-volume ratio) to conventional rectangular designs. Coupled to methacrilate devices, rhomboidal chips offered reproducible 100% insertion and 95% extraction yields, rivaling those obtained with serpentine-like chips and confirming that chamber design is a key factor in determining sample insertion and extraction yields.

As mentioned above, serpentine-like PCR-chambers, first reported in flow-through PCR by Kopp [38] and later analyzed by Scheneegaβ [18], are of relevance due to their superior insertion/extraction rates. However, in a non flow-through scheme serpentine-like designs could also, in principle, affect chip PCR through changes in the surface-to-volume ratio or by altering reaction kinetics. Unfortunately, the work by Kopp and Scheneegaβ involves pressure-pumped flow PCR through a multi-temperature serpentine (rather than uniform heating of a static PCR-mix) and, thus, it does not provide information about the effects of serpentine chambers on reaction kinetics when conducting static PCR. Later work has made use of static serpentine chambers [22], but no comparative data with rectangular chambers is provided. In this work we conducted repeated experiments with rhomboidal and serpentine-like PCR-chips. The results (see Figure 9) indicate that, with the titrated amount of BSA adjuvant here used (2.5 μg/μl), no apparent differences can be observed between the PCR-products of both designs, suggesting that PCR efficiency is not hampered by kinetic effects on a serpentine-like chamber. On the contrary, the smaller chamber volume of the here reported serpentine PCR-chips (18.7 μl) hints at a probable superior efficiency of PCR in these systems, even though their surface-to-volume ratio (13.98 mm^{-1}) is slightly higher than that of rhomboidal PCR-chips (11.82 mm^{-1}). The combination of these results with insertion/extraction yields, and with a presumably more amenable design for integration into pressure-pumped microsystems, makes serpentine-like chamber design an obvious candidate for the future development of PCR-chips.

3.3. Temperature control systems

Temperature control is a tough problem in PCR and the way it is dealt with determines many aspects of a PCR micro-device (e.g. external vs. integrated heaters). Although PCR can be carried out with relatively low accuracy (±1.5 ºC, [4]), the perceived wisdom is that a more precise temperature control will improve both reaction yields and specificity [14]. To achieve the ±0.2 ºC precision here reported we examined several issues concerning the design of the temperature control system for both passive and active PCR-chips. A first issue concerning temperature control refers, precisely, to how this control is implemented. From a kinetics point of view, temperature control in a PCR-chip is not straightforward, since two opposing effects (very fast transients and very stable holds) are sought in chip PCR operation. When documented, reported control methods consist of simple PID [22, 23] or PI [32] algorithms implemented mostly by software. However, given the low thermal mass of active PCR-chips and the fast transients sought, the integral term of simple PID/PI control will tend to cause overshoots that can be, particularly at denaturing temperatures, severely detrimental to PCR. In this work, we developed a two-step control method to take advantage of full PID stability without incurring in the aforementioned overshoots. By means of an adjustable hysteresis, a PD control was used to generate fast heating and cooling ramps, while a full PID control took over only during temperature holds. With this dual PD-PID scheme, we were able to provide very fast transients (up to 15 ºC/s) in active PCR-chips, with minimal overshooting (below 0.2 ºC) and very stable temperature holds (maximum deviations of ±0.2 ºC, see Figure 8).

Guaranteeing a homogeneous temperature distribution across the PCR chamber is also an essential requisite in PCR-chips. In passive PCR-chips, homogenous heat distribution is typically achieved through the placement of an oxygen-free copper block between the underlying Peltier cell and the PCR-chip [15, 17]. However, the introduction of a copper block imposes a severe limit on the transient capabilities of the system and on the time

required for temperature stabilization if temperature overshoots are to be avoided. Here we examined the causes of the non-homogeneity Peltier cells display on their surface and the minimum copper block thickness required to overcome it. A Peltier cell consists of an array of parallel PN junctions (typically Bi_2Te_3 junctions) and since, for a set voltage, each parallel PN junction of the Peltier cell establishes its own temperature differential, the Peltier cell will invariably tend to create a radial temperature gradient on its hot surface. This gradient can rise up to 2.5 ºC for 30x30 mm Peltier cells (see Figure 11), strongly hindering PCR efficiency. Thus, an oxygen-free copper block is necessary to redistribute heat in centimeter-sized chips, and can only be discarded (to improve transients) when using smaller chips and/or cells [16, 33]. For the Peltier cell used in this work we found out that 1 mm-thick copper blocks (with 0.5 ºC gradients) were the most suitable choice, since 0.5 mm-thick blocks still presented up to 1 ºC gradients and 2 mm-thick blocks slowed transients excessively without improving gradients (0.4 ºC) in a remarkable way.

Similarly, homogenous temperature distribution in active PCR-chips is also critical to achieve efficient and specific reactions. In this context, the inter-digitized design here reported (see Figure 3) introduces many advantages over conventional approaches. On the one hand, the parallel actuator grid ensures by design a homogenous distribution of the applied heat over the whole PCR-chamber, since all heating elements contribute equally across the reservoir length. In turn, the inter-digitized parallel sensor grid provides an average measurement of the PCR-chamber temperature, thus avoiding the sensing problems posed by the formation of air bubbles when using localized platinum resistor sensors [23, 30]. Moreover, the parallel resistor grid design here implemented results in fault-tolerant heating and, to a lesser degree, sensing systems, since accidental breakage or misbehavior of an individual resistor element is automatically compensated by the parallel nature of the grid. On the other hand, the use of a single polysilicon layer for the creation of heater and sensor elements minimizes the complexity of the underlying technological process, since it avoids the use of additional metal layers (such as Pt) and lift-off processes that are not fully compatible with standard CMOS. The low TCR, close to that of most thin-film materials used for temperature sensing, and the high linearity of standard CMOS polysilicon layers over PCR temperature ranges (see Figure 5) guarantee that an accurate temperature control (±0.2 ºC) can be achieved while using only CMOS-compatible materials and processes. This exclusive use of CMOS-compatible processes is significant, since it introduces the possibility of integrating control and optical or electrical detection circuitry [35, 36, 39] on the same PCR-chip. It should be noted that single-layer polysilicon systems have already been described for CMOS-compatible PCR-chips [4]. However, and in contrast with previous schemes, the inter-digitized sensor-heater design here reported provides independent sensors and actuators in a single layer, and thus does not require the use of the same serpentine-like element [4] both as sensor and actuator, a strategy that imposes an upper limit to the temperature precision attainable with single layer systems.

3.4. System comparison

Another interesting item of PCR-chips that has not been directly contrasted previously concerns the integration of thermocycling elements. Although integrated thin-film heaters were introduced first [4], most subsequent research on PCR-chips has been carried out using external Peltier cells [15-17, 22, 33] and, even though integrated heaters have been taken up thereafter [18, 21, 23, 32, 35, 36], no direct comparison between both systems is available in the literature. Taking into account the significant implications on design, prototyping and production that choosing between both these alternatives can have, here we undertook a straight comparison of both systems in terms of PCR-product efficiency, speed and power consumption. As it is to be expected from their lower thermal mass, active PCR-chips outperform passive ones in terms of speed and power consumption (see Figure 12). On average, when using optimized PCR-protocols, passive PCR-chips (with the Peltier cell cold side at 55 ºC) yielded 5 ºC/s heating and cooling rates and a mean power consumption of 12.3 W, whilst active PCR-chips provided remarkably higher heating rates (up to 15 ºC/s) and similar cooling rates (5 ºC/s) with an average power consumption of

just 2.8 W. The greater heating and cooling rates of active PCR-chips resulted in a net difference of global analysis times between both kinds of systems. This difference peaked when very fast PCR-protocols (in which most time is spent in transitions, see Figure 8) were implemented, leading to 15-20% shorter analysis times in active PCR-chips.

In contrast, active PCR-chips did not outperform passive ones in terms of PCR-product efficiency. Straight comparison of amplification results using identical PCR-protocols (see Figure 13) shows slightly superior PCR performance in passive PCR-chips. A feasible explanation for this effect can be sought in the poorer transition rates and the slightly heavier temperature overshoots (see Figure 12) of passive PCR-chips. Slower transitions and longer stabilization times due to increased overshoots generate prolonged extension and annealing periods both during the temperature stabilization phase and the initial stages of transition. Since Taq polymerase is partially active (some two orders of magnitude less) at annealing temperatures and annealing may begin to take place (depending on primer length and composition) up to 5 ºC off the estimated annealing temperature [31], both factors can significantly contribute to an increase of PCR efficiency (though at the loss of some specificity). Evidence for this line of reasoning comes also from the fact that the superiority in performance of passive PCR-chips increased as faster PCR-protocols were implemented (data not shown). Faster PCR protocols (see Figure 8) entail shorter hold times and, thus, small additions to either annealing or extension periods can significantly contribute to overall performance. In addition, Peltier cells present non-irrelevant temperature deviations (up to 0.5 ºC, see above) across their hot surfaces that can also contribute to promote additional primer annealing. Even if primers have carefully been chosen to avoid efficiency loss due to low annealing rates in fast PCR operation, a perfect match of annealing temperatures between both primers is rather difficult to obtain and slight temperature variations during the annealing period may contribute to enhance primer annealing and, thus, PCR efficiency. This could be certainly the case for the work here reported, where the difference between primers annealing temperatures was in the whereabouts of 0.3 ºC.

In the light of these results, the debate over which thermocycling system is best suited for PCR-chips remains certainly open and application-dependant. Active PCR-chips present far better speed and power consumption rates, and these may be highly desirable in certain applications, like portable PCR [40] or rapid pathogen detection [41] systems. In addition, the integration of heating circuitry provides a more scalable technology for the development of multi-chip modules or the integration of additional mechanisms (e.g. sensors or control circuitry). Passive PCR-chips, in turn, provide easier prototyping and a slightly superior performance, but it remains to be seen whether this difference in efficiency would hold if chip dimensions were shrunk [33] and smaller and faster Peltier cells (with lower thermal masses) were used.

4. Conclusion

In the present work we have shown that fully functional PCR-chips with similar capabilities to those previously described can be produced using solely CMOS-compatible materials and processes. Polysilicon resistor sensors and heaters have been integrated in a single layer and characterized, providing ample heating (up to 20 ºC/s) and accurate sensing (± 0.1 ºC) capabilites. The ensuing PCR-chips have been tested over a wide range of templates and protocols, and PCR kinetics and mixtures have been optimized for PCR-chip operation, leading to reproducible PCR amplifications in 20 min (~24.41 s/cycle) using very low Taq polymerase (0.056 U/μl) and template DNA (2.4 ng/μl) concentrations. The developed PCR-chip platform has been used as a common reference ground to conduct the first full-fledged analysis of many different PCR-chip design and system strategies. From the reported results, several conclusions may be drawn. On the one hand, sample insertion and extraction yields have been shown to be extremely dependent on chip design and coupling machinery, with the highest extraction yields (above 95%) corresponding to serpentine-like chips, but followed closely by the here introduced rhomboidal reservoir design. In this regard, the influence of static serpentine-like chamber designs over PCR efficiency has been assessed and it has been found that this design option does not hinder

PCR in a noticeable manner. On the other hand, Peltier and integrated-heater driven systems have been functionally compared for the first time. As expected, integrated-heater chips yield lower power consumption and analysis times, but at the expense of a slightly lower efficiency that can be attributed to their more precise operation. Finally, the reported single use of CMOS-compatible processes enables a fast and ready production of these systems in most available foundries and paves the way for a future integration of detection and control circuitry in PCR-chips.

Acknowledgements

This work was partly funded by the Consejo Superior de Investigaciones Científicas (CSIC), by Grant TIC97-0569 from the Comisión Interministerial de Ciencia y Tecnología (CICYT) and by Grants BMC2001-2065 from the Ministerio de Ciencia y Tecnología (MCyT) de España and 2001SGR-206 from the Departament d'Universitats, Recerca i Societat de la Informació (DURSI) de la Generalitat de Catalunya.

References

[1] Manz, A., Harrison, D. J., Verpoorte, E. M. J., Fettinger, J. C., Paulus, A., Lüdi, H., Widmer, H. M., 1992. Planar chips technology for miniaturization and integration of separation techniques into monitoring systems. Capillary electrophoresis on a chip. *J. Chrom.* **593**, 253-258.

[2] Austin, R. H., Volkmuth, W. D., 1993. Electrophoresis and microlithography, *Analusis* **21**, 235-238.

[3] Woolley, A. T., Mathies, R. A., 1994. Ultra-High-Speed DNA Fragment Separations Using Microfabricated Capillary Array Electrophoresis Chips, *Proc. Natl. Acad. Sci. USA* **91**, 11348-11352.

[4] Northrup, M. A., Ching, M. T., White, R. M., Watson, R. T., 1993. DNA amplification in a microfabricated reaction chamber, in *Digest of technical papers: Transducers 1993 (Proc. 7th International Conference on Solid-State Sensors and Actuators)*, 924-926.

[5] Fodor, S. P. A., Rava, R. P., Huang, X. C., Pease, A. C., Holmes, C. P., Adams, C. L., 1993. Multiplexed biochemical assays with biological chips, *Nature* **364**, 555-556.

[6] Burns, M .A., Johnson, B. N., Brahmasandra, S. N., Handique, K., Webster, J. R., Krishnan, M., Sammarco, T. S., Man, P. F., Jones, D. K., Heldsinger, D., Mastrangelo, C. H., Burke, D. T., 1998. An integrated nanoliter DNA analysis device, *Science* **282**, 484-487.

[7] Anderson, R. C., Su, X., Bodgan, G. J., Fenton, J., 2000. A miniature intetgrated device for automated multistep genetic analysis, *Nucl. Acids Res.* **28**, e60, i-vi.

[8] Belgrader, P., Okuzumi, M., Pourahmadi, F., Borkholder, D. A., Northrup, M. A., 2000. A microfluidic cartridge to prepare spores for PCR analysis. *Biosens. Bioelec.* **14**, 849-852.

[9] Lagally, E. T., Medintz, I., Mathies, R. A., 2001. Single-molecule DNA amplification and analysis in an integrated microfluidic device. *Anal. Chem.* **73**, 565-570.

[10] Cheng, J., Shoffner, M. A., Mitchelson, K. R., Kricka, L. J., Wilding, P., 1996. Analysis of ligase chain reaction products amplified in a silicon-glass chip using capillary electrophoresis, *J. Chromatogr.* **732**, 151-158.

[11] Radtkey, R., Feng, L., Muralhider, M., Duhon, M., Canter, D., DiPierro, D., Fallon, S., Tu, E., McElfresh, K., Nerenberg, M., Sosnowski, R., 2000. Rapid high fidelity analysis of simple sequence repeats on an electronically active DNA microchip. *Nuc. Acids Res.* **28**, e17, i-vi.

[12] Westin, L., Xu, X., Miller, C., Wang, L., Edman, C.F., Nerenberg, M., 2000. Anchored multiplex amplification on a microelectronic chip array. *Nat. Biotechnol.* **18**, 199-204.

[13] de Mello, A. J., 2001. DNA amplification: does 'small' really mean 'efficient'? *Lab Chip*, **1**, 24N-29N.

[14] Wittwer, C. T., Fillmore, G. C., Garling, D. J., 1990. Minimizing the time required for DNA amplification by efficient heat transfer to small samples, *Anal. Biochem.* **186**, 328-331.

[15] Wilding, P., Shoffner, M. A., Kricka, L. J., PCR in silicon microstructure, 1994. *Clin. Chem.* **40**, 1815-1818.

[16] Taylor, T. B., Winn-Deen, E. S., Picozza, E., Woudenberg, T. M., Albin, M., 1997. Optimization of the performance of the polymerase chain reaction in silicon-based structures, *Nucl. Acids Res.* **25**, 3164-3168.

[17] Shoffner, M. A., Cheng, J., Hvichia, G. E., Kricka, L. J., Wilding, P., 1996. Chip PCR. I. Surface passivation of microfabricated silicon-glass chips for PCR, *Nucl. Acids Res.* **24**, 375-379.

[18] Schneegaß, I., Bräutigam, R., Köhler, J. M. 2001. Miniaturized flow-through PCR with different template types in a silicon chip thermocycler, *Lab Chip*, 1, 42 – 49.
[19] Erill, I., Campoy, S., Erill, N., Barbé, J., Aguiló, J., 2003. Biochemical analysis and optimization of inhibition and adsorption phenomena in glass-silicon PCR-chips, *Sens. Act. B.* **96**, 685-692.
[20] Burns, M. A., Mastrangelo, C. H., Sammarco, T. S., Man, F. P., Webster, J. R., Johnson, B. N., Foerster, B., Jones, D., Fields, Y., Kaiser, A. R., Burke, D. T., 1996. Microfabricated structures for integrated DNA analysis *Proc. Natl. Acad. Sci. USA* **93**, 5556-5561.
[21] Poser, S., Schulz, T., Dillner, U., Baier, V., Köhler, J. M., Schimkat, D., Mayer, G., Siebert, A., 1997. Chip elements for fast thermocycling, *Sens. Act. A* **62**, 672-675.
[22] Lin, Y. -C., Huang, M. -Y., Young, K. -C., Chang, T. -T., Wu, C. -Y., 2000. A rapid micro-polymerase chain reaction system for hepatitis C virus amplification, *Sens. Act. B* **71**, 2-8.
[23] Zhan, Z., Dafu, C., Zhongyao, Y., Li, W., 2000. Biochip for PCR amplification in silicon, *Proc. 1st Annual International IEEE-EMBS Special Topic Conference on Microtechnologies in Medicine & Biology*, 25-28.
[24] Merlos, A., Acero, M.C., Bao, M.H., Bausells, J., Esteve, J., 1993. TMAH/IPA Anisotropic etching characteristics, *Sens. Act. A* **37-38**, 737-743.
[25] Wallis, G., Pomerantz, D.I., 1969. Field assisted glass-metal sealing, *J. Appl. Phys.* **40**, 3946-3949.
[26] Plaza, J. A., Esteve, J., Lora-Tamayo, E., 1998. Effect of the silicon oxide, silicon nitride and polysilicon layers on the electrostatic pressure during the anodic bonding, *Sens. Act. A* **67**, 181-184.
[27] Jönsson, U., Ivarsson, B., Lundström, I., Berghem, L., 1982. Adsorption behavior of fibronectin on well-characterized silica surfaces, *J. Colloid Interface Sci.* **90**, 148-163.
[28] Tartof, K. D., Hobbs C. A., 1987. Improved media for growing plasmid and cosmid clones, *Bethesda Res. Lab. Focus.* **9**, 12.
[29] Sambrook, J., Fristch, E. F., Maniatis, T., 1989. *Molecular cloning. A laboratory manual, 2nd Ed.* Cold Spring Harbor Laboratory Press.
[30] Lin, Y. -C., Yang, C. -C., Huang, M. -Y., 2000. Simulation and experimental validation of micro polymerase chain reaction chips, *Sens. Act. B* **71**, 127-133.
[31] Innis, M. A., Gelfand, D. H., 1990. Optimization of PCRs, in Innis, M. A., Gelfand, D. H., Sninsky, J. J., White, T. J. (Eds), *PCR Protocols - A guide to methods and applications*, Academic Press.
[32] Yoon, D. S., Lee, Y-S., Lee, Y., Cho, h. J., Sung, S. W., Oh, K. W., Cha, J., Lim, G. 2002. Precise temperature control and rapid thermal cycling in a micromachined DNA polymerase chain reaction chip, *J. Micromech. Microeng.* **12**, 813-823.
[33] Murakami, Y., Nagai, H., Kikuchi, T., Yamamura, A., Idegami, K., Yanase, M., Choi, Y. -S., Morita, Y., Tamiya, E., 2000. Random distribution of biomaterials as a handling method on microarray applied to PCR, biosensors and high-throughput screening, *Proc. 1st Annual International IEEE-EMBS Special Topic Conference on Microtechnologies in Medicine & Biology*, 29-33.
[34] Wittwer, C. T., Reed, G. B., Ririe, K. M. 1994. *The polymerase chain reaction*, Ed. Mullis, K. B., Ferré, F., Gibbs, R. A. Birkhauser, Boston, 174-181.
[35] Namasivayam, V., Lin, R., Johnson, B., Brahmasandra, S., Razzacki, Z., Burke, D. T., Burns, M. A. 2004. Advances in on-chip photodetection for applications in miniaturized genetic analysis systems, *J. Micromech. Microeng.* **14,** 81-90.
[36] Schabmueller, C. G. J., Pollard, J. R., Evans, A. G. R., Wilkinson, J. S., Ensell, G., Brunnschweiler, A. 2001. Integrated diode detector and optical fibres for in situ detection within micromachined polymerase chain reaction chips, *J. Micromech. Microeng.* **11**, 329-333.
[37] Woolley, A. T., Hadley, D., Landre, P., deMello, A. J., Mathies, R. A., Northrup, M. A., 1996. Functional integration of PCR amplification and capillary electrophoresis in a microfabricated DNA analysis device, *Anal. Chem.* **68**, 4081-4086.
[38] Kopp, M. U., de Mello, A. J., Manz, A., 1998. Chemical amplification: continuous-flow PCR on a chip, *Science* **280**, 1046-1048.
[39] Gabig-Ciminska, M., Holmgren, A., Andresen, H., Bundvig Barken, K., Wümpelmann, M., Albers, J., Hintsche, R., Breitenstein, A., Neubauer, A., Los, M. *et al.* 2004. Electric chips for rapid detection and quantification of nucleic acids, *Biosens. Bioelec.*, **19**, 537-546.
[40] Northrup, M. A., Benett, B., Hadley, D., Landre, P., Lehew, S., Richards, J., Stratton, P., 1998. A miniature analytical instrument for nucleic acids based on micromachined silicon reaction chambers, *Anal. Chem.* **70**, 918-922.

[41] Belgrader, P., Benett, W., Hadley, D., Long, G., Mariella, R., Milanovich, F., Nasarabadi, S., Nelson, W., Richards, J., Stratton, P., 1998. Rapid pathogen detection using a microchip PCR array instrument, *Clin. Chem.* **44**, 2191-2194.

Figures and legends

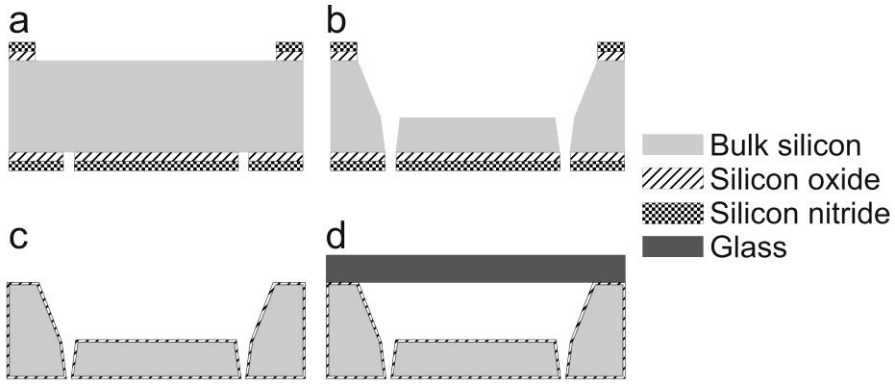

Figure 1. Technological process for passive PCR-chips. PCR-chamber and access holes definition (a), front and back side etches (b), silicon oxide passivation (c) and anodic bonding to glass (d).

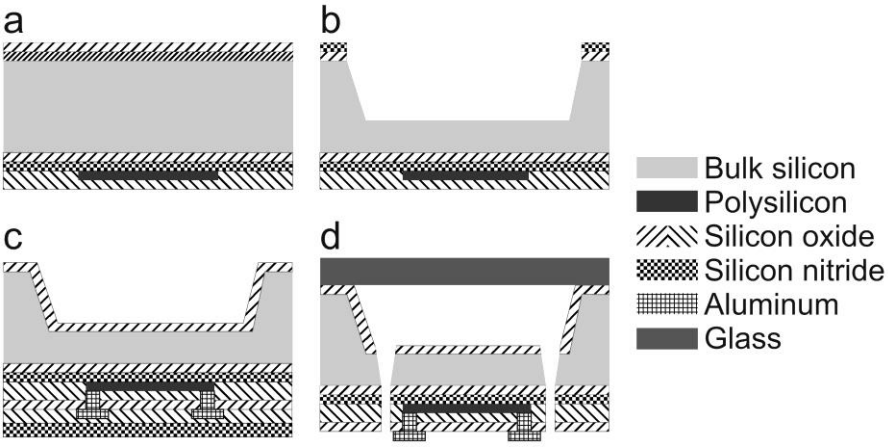

Figure 2. Technological process for active PCR-chips. Polysilicon resistor definition (a), PCR-chamber etch (b), contact pads and insulation (c) and access holes etch plus anodic bonding (d).

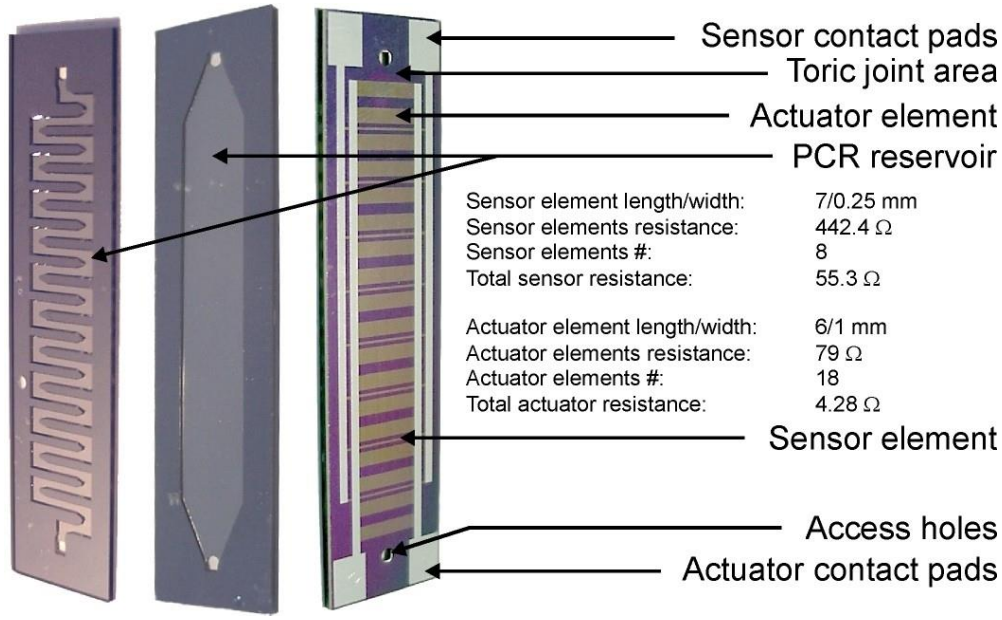

Figure 3. Front (serpentine and rhomboidal) and rear view of active PCR-chips showing the inter-digitized parallel grid of sensor and actuator polysilicon resistors. Serpentine reservoir: 152.95 x 0.7 x 0.175 mm^3 ~ 18.73 µl. Rhomboidal reservoir: 29 x 5 x 0.175 mm^3 ~ 25.37 µl. Chip dimensions: 40 x 10 x 0.8 mm^3.

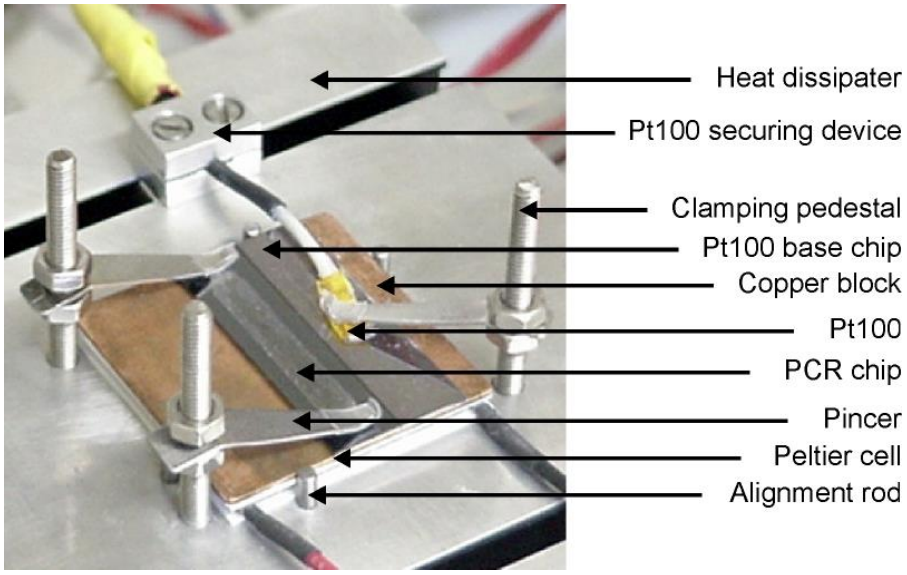

Figure 4. System setup for passive PCR-chips. The PCR-chip and the Pt100 sensor are clamped with Teflon insulated pincers onto silicon oxide passivated base chips.

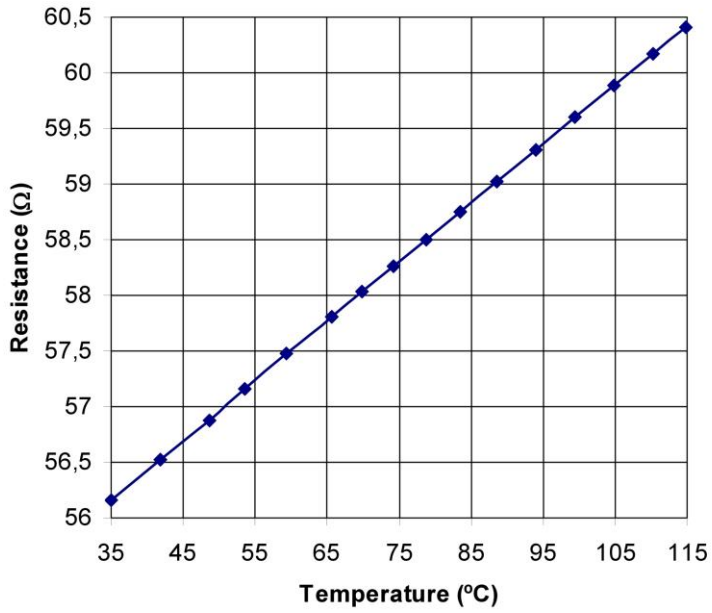

Figure 5. Plot of polysilicon sensor grid read-resistance vs. reference thermometer temperature. As it can be seen, the polysilicon resistor grid presents high linearity on the PCR temperature range and read-resistance could be easily converted to temperature readings with a 3rd degree polynomial interpolator.

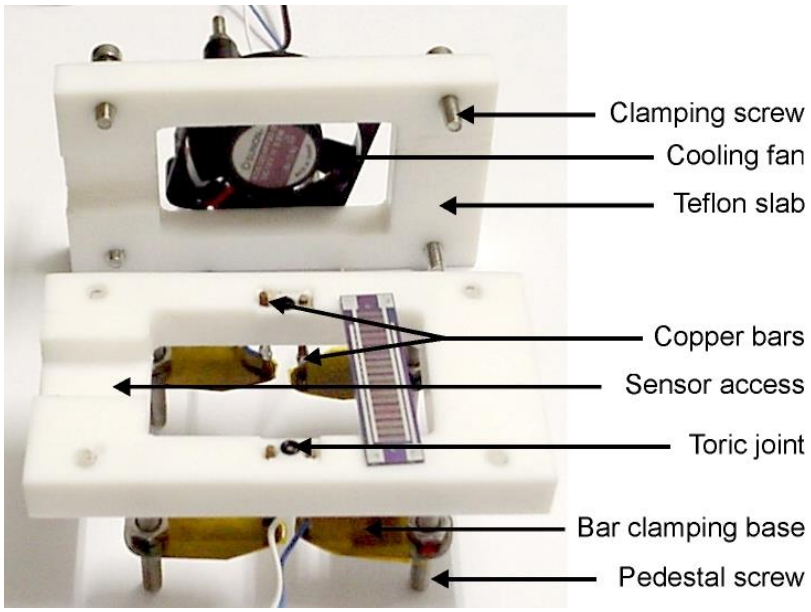

Figure 6. Custom Teflon device for active PCR-chips. Toric joints provide airtight sealing, while pedestal screws act both as base for the system and as clamping support (through Teflon insulated bases) for electrical contact copper bars. The chip is placed on the grinded surface of the lower slab (flipped with reference to the picture), with the electrical pads making contact with the copper bars and the access holes coupled to the toric joints for airtight sealing.

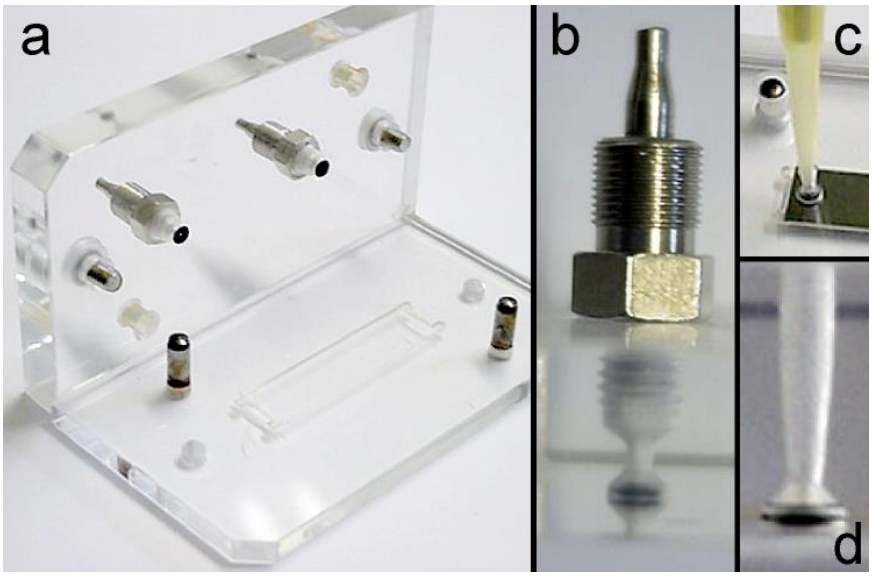

Figure 7. Insertion/extraction and washing methacrilate devices. General view of a washing device (a), cross-section of a washing device port (b) and close view (c) and cross-section (d) of the insertion/extraction device and one of its pipette-tip shaped holes.

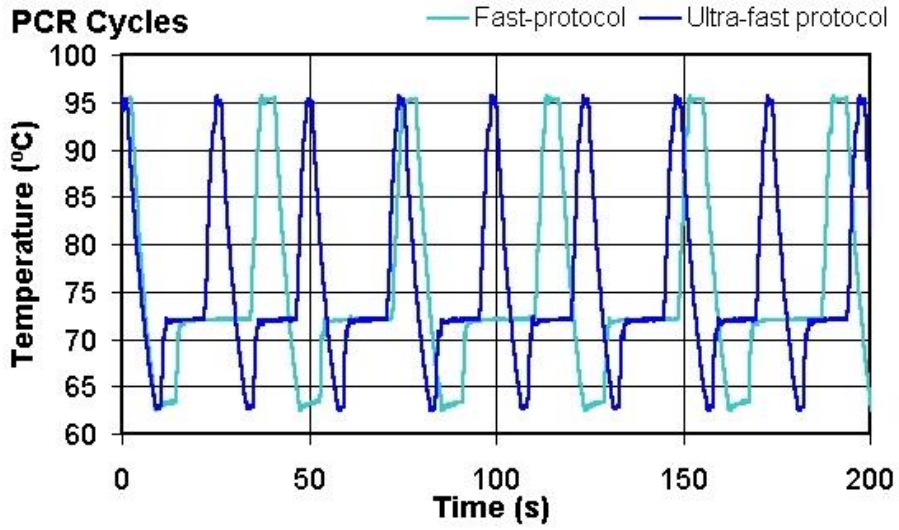

Figure 8. PCR cycles for the fast (S_N, R_N) and ultra-fast (R_{UFast}, see Fig. 8) PCR protocols in active PCR-chips. Fast PCR protocol: 95.5 ºC – 1 min, (95.5 ºC – 3 s, 64 ºC – 7 s, 72 ºC – 17 s) x 45, 72 ºC –1 min. Fast analysis time: 30:28 min; cycle time: 38 s. Ultra-fast PCR protocol: 95.5 ºC – 1:30 min, (95.5 ºC – 1 s, 64 ºC – 2 s, 72 ºC – 10 s) x45, 72 ºC – 30 s. Ultra-fast analysis time: 20:19 min; cycle time: 24.41 s. Thermal cycler control analysis time: 56:43 min. Active PCR-chip average heating rate: 10.73 ºC/s; average cooling rate: 5.6 ºC/s.

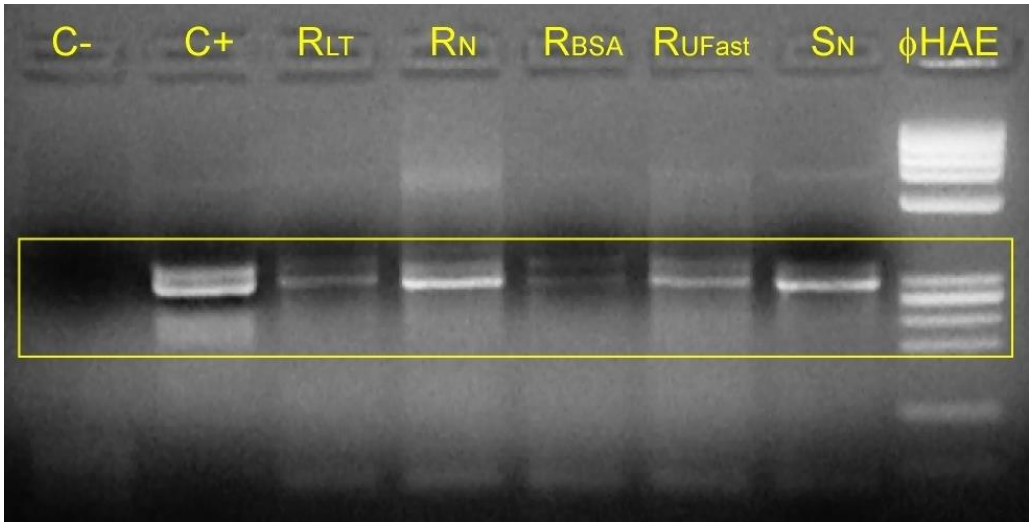

Figure 9. Agarose gel of PCR-products using different active PCR-chips and protocols (see Figure 8). *C+* and *C-* lanes correspond, respectively, to positive and negative controls run on a Mastercycler personal (*Eppendorf*) thermal-cycler (~1 h). R_N and S_N lanes correspond to fast PCR experiments (~30 min) using standard conditions with either rhomboidal (*R*) or serpentine-like (*S*) chips, while R_{LT} and R_{BSA} correspond, respectively, to fast PCR assays using a halved concentration of Taq polymerase (0.028 U/μl) and this same concentration of Taq with a doubled concentration of BSA (5 μg/μl). The R_{UFast} lane corresponds to an ultra-fast assay (~20 min) with a doubled template-DNA concentration (4.8 ng/μl). Secondary structures, indicative of low specificity, can be observed in the positive control lane (*C+*), but disappear in chip experiments, evidencing an improved specificity. Conversely, the amount of PCR product is slightly greater in the positive control, and can be seen to decrease from PCR-chip standard experiments (R_N and S_N) as faster cycling is imposed (R_{UFast}) or Taq polymerase concentration is decreased (R_{LT}, R_{BSA}).

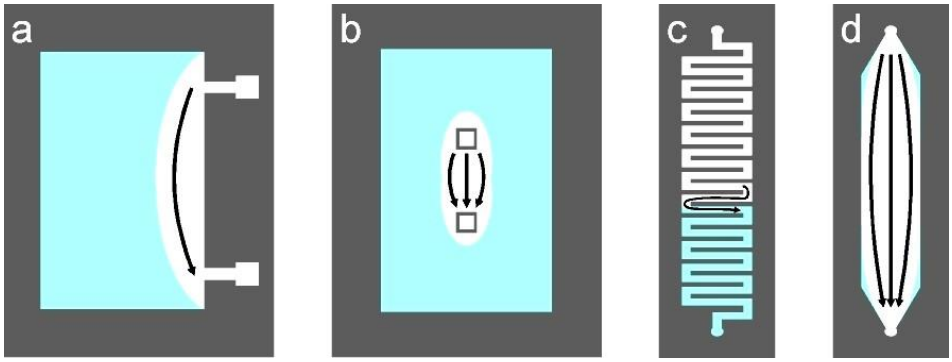

Figure 10. Examined PCR-chip designs and their liquid stacking problems. Arrows represent air (white) flow. As the cross-sectional area of the PCR-chamber decreases (*d* and, particularly, *c*), liquid stacking (light gray) is minimized and extraction yields improve accordingly.

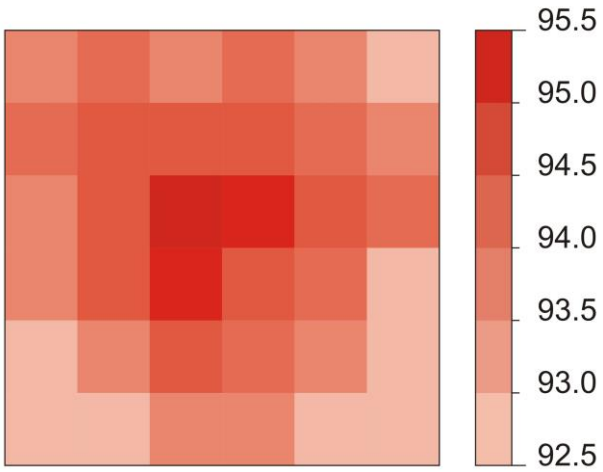

Figure 11. Temperature distribution across the CP 1.0-127-05L Peltier cell hot side surface, as averaged from three independent experiments in which 36 temperature readings were taken with a clamped Pt100 sensor after a 20 min stabilization period at 95 °C.

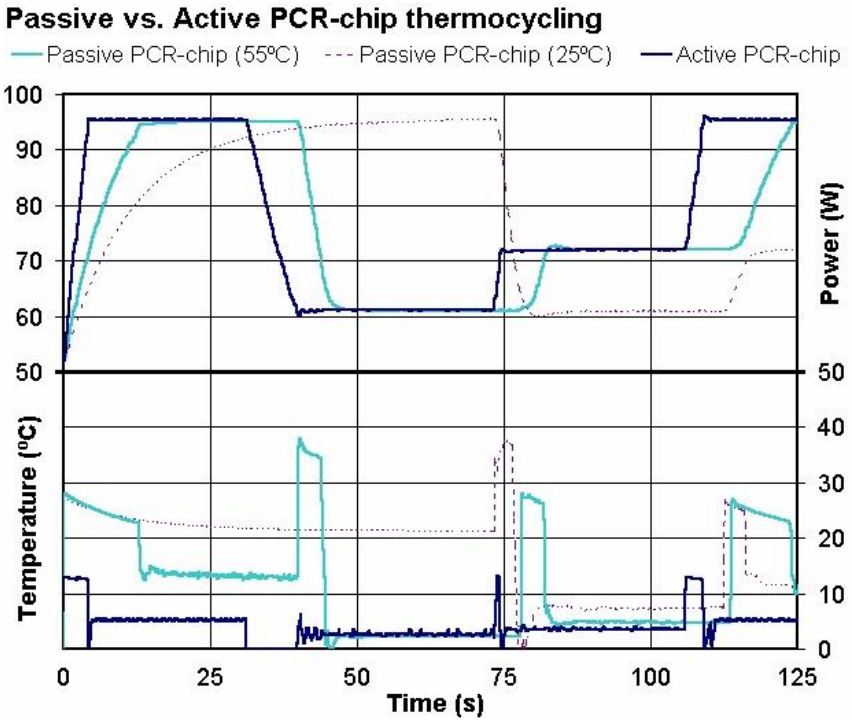

Figure 12. Comparison of cycling speed and power consumption between passive (Peltier cell driven) and active PCR-chips during a typical PCR cycle. As it can be observed, active PCR-chips (dark gray) cycle faster and consume far less during rise ramps (~12 W) and holds (5.4 – 2.3 W) than their passive (light gray) counterparts (25 W and 13 – 5 W, respectively), while not consuming at all during cooling, in which Peltier cells display huge power consumption (34 W). With the Peltier cell cold side at ambient temperature (dotted line), performance diminishes dramatically and power consumption rises during hold periods. Average power consumption: 11.3 W for passive PCR-chips (Peltier cold side at 55 °C) and 3.7 W for active PCR-chips. Average rise and fall rates: 3.2 and 6.8 °C/s for passive PCR-chips; 10.5 and 4.3 °C/s for active PCR-chips.

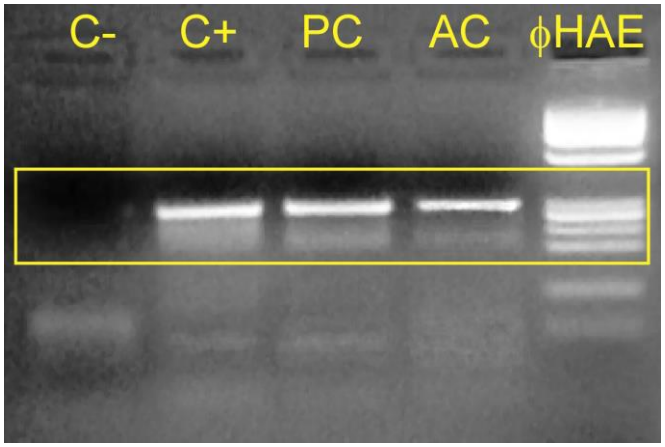

Figure 13. Agarose gel of PCR-products using passive and active PCR-chips and the above described PCR protocol. *C+* and *C-* lanes correspond, respectively, to positive and negative controls run on a Mastercycler personal (*Eppendorf*) thermal-cycler (~1:43 h). The *PC* lane corresponds to a passive PCR-chip experiment with the Peltier cold side at 55 ºC (~69 min), while the *AC* lane corresponds to an active PCR-chip product (~56 min). A slight difference in PCR efficiency between passive and active PCR-chips can be observed, with the former producing yields comparable to those of positive controls.